

Numerical Investigation of the Local Shear Rate in a Twin-Screw Extruder for the Continuous Processing of Li-Ion Battery Electrode Slurries

Juan Fernando Meza Gonzalez* and Hermann Nirschl

The mixing step for electrode slurry preparation in the manufacture of batteries is highly relevant because it directly affects the downstream production processes and the performance of the battery cells. In this work, a study of the flow behavior and material strain in a twin-screw extruder is carried out to analyze its efficiency for continuous battery slurry processing. Here, individual elements of the extruder screw are simulated using the smoothed particle hydrodynamics method. Based on the resulting flow profiles, a dimensionless analysis is used to validate the calculations. Hence, the local shear rate and pressure profiles are evaluated for different screw geometries. The effects of the screw design and process setup are discussed, to accordingly improve the mixing process.

1. Introduction

Batteries are commonly used as a local energy storage solution to facilitate off-grid power usage or as an on-demand energy power source. The growing interest in novel battery solutions for more energy intensive applications is driving the development of agile production processes, capable to adapt to new technologies requirements. Accordingly, new battery materials are constantly being developed to improve the electrochemical properties of battery cells, with the intention to create efficient batteries for both high power and high-performance applications.^[1,2]

The production of battery cells involves multiple processing steps: starting from the mixing process, where the electrode components are combined to form viscous slurries for easier processing of the materials, succeeded by the electrodes fabrication, where current-collector sheets are coated with the electrode slurries, then dried and calendered to form electrode sheets, and

finally, they are cut and processed into battery packs.^[2,3] Each process in the chain affects the performance of the cells in a certain way. Consequently, changes in a single processing step may introduce large discrepancy into the final product quality. Battery production lines rely on precise processing methods to constantly achieve high battery quality. Thus, understanding the relationship between processing parameters and cell performance is of great interest in order to optimize production lines.^[2]

Numerical models are an excellent tool for predicting and analyzing quality changes of the electrodes during production. Various numerical methods can be

applied to help characterize and optimize each processing step depending on the application. It allows the analysis of the performance of the process and the effects on the products prior to performing experiments.^[4–6] Most of these models rely on different simulation methods to analyze structural changes of the electrodes based, for example, on particles simulations.^[4] Considering the mixing step, the discrete element method (DEM) is commonly used to simulate dry mixing of components. In the case of wet mixing, simulations require the implementation of shear forces, which have a significant impact on accuracy and computational cost depending on the application.^[4,7,8] Another approach will be the implementation of multiscale simulation tools. Ngandjong et al.^[5] and Rucci et al.^[6] proposed a solution based on coarse-grained molecular dynamics to correlate various processing steps with the electrochemical performance of the batteries. In these studies, however, the electrode slurries are modeled by randomly generated distributions of particles, which do not fully incorporate the mixing step.

The mixing step in the battery cells production directly affects the downstream processes and the performance of the battery cells.^[2,4] It adjusts the product quality by determining the particle size distribution and the homogeneity of the electrodes, which has been found to be fundamental for the electrochemical properties of the battery cells.^[4,9,10] Moreover, it defines the rheological properties of the slurries, affecting directly its processability in the following production steps.^[2,4]

The development of a mixing process capable of handling different materials is of great interest, especially in matters of flexible production rates, without compromising product quality and minimizing waste. This also affects the scalability of the process.^[2] Battery slurries are commonly produced in batch processing machines such as planetary mixers or high speed mixer

J. F. Meza Gonzalez, H. Nirschl
Institute of Mechanical Process Engineering and Mechanics
Karlsruhe Institute of Technology
Strasse am Forum 8, 76131 Karlsruhe, Germany
E-mail: juan.meza@kit.edu

 The ORCID identification number(s) for the author(s) of this article can be found under <https://doi.org/10.1002/ente.202201517>.

© 2023 The Authors. Energy Technology published by Wiley-VCH GmbH. This is an open access article under the terms of the Creative Commons Attribution-NonCommercial-NoDerivs License, which permits use and distribution in any medium, provided the original work is properly cited, the use is non-commercial and no modifications or adaptations are made.

DOI: 10.1002/ente.202201517

(dissolver).^[2,7,11] These types of processes are reliable but limited in their flexibility as they are not suitable for variable production rates. A continuous mixing approach is therefore more attractive to enhance flexibility.^[2] A comparison regarding battery slurry preparation based on continuous and discontinuous process was shown by Dreger et al.^[11] Here, the extrusion process stands out due to its improvement of the electrochemical properties of Li-ion batteries as well as cost-efficiency and scalability, especially when handling high solid contents.

In this work, a twin-screw extruder (TSE) is evaluated as a continuous mixing solution for scalable battery production lines. A continuous process reduces waste in battery slurry preparation. It also provides the flexibility to formulate small and large batches of slurry with similar mechanical stress.^[2] Extruders have multiple degrees of freedom when it comes to mixing applications, due to its flexibility in screw geometry arrangement and control in processing sequence of materials.^[2] The mixing performance of these devices needs to be analyzed in order to efficiently adapt the process to the production of battery slurries. The evaluation of different process parameters in a digital framework provides the advantage of reducing the laboratory experiments needed to characterize the process. Additionally, the generated data can be used to fully understand experimental results and estimate changes inside the process. Extruders usually have temperature and torque sensors for monitoring product quality during the process; however, this only describes mechanical stress provided by the device in general. In addition, measuring product quality during extrusion is difficult due to the construction of the machines and is usually only possible at the end of the extruder. Through flow simulations of the process, a more detailed analysis of the material processing features can be achieved. Moreover, a numerical investigation also enables a local characterization of the material response to process changes, especially considering particle breakage induced by the process.^[4,8] In the work of Asylbekov et al.,^[8] the breaking behavior of aggregates found in Li-Ion batteries while mixing is analyzed. Here, the relevance of shear stress-induced particle breaking is introduced. The evaluation is based on DEM simulations of cathode processing in a planetary mixer, where the importance on aggregate size and critical shear stress to promote aggregate fracturing is denoted. As shearing is strongly present in extruders,^[2] the analysis of the shear stress in extruders accounts as a crucial efficiency factor to be investigated in order to understand and characterize the deagglomeration rates in this continuous device.^[4]

With the performed simulations, the authors aim to introduce a numerical characterization approach of the mixing process to quantify the material strain induced by the extruder. Additionally, through analysis of the reproduced flow states in the extruder, the effects of different combinations of process parameters are discussed in order to provide a description of the shear rates and dispersion during the process.

2. Process Simulation

The aim of this work is to develop a digital framework for analysis and proper process design of a continuous battery slurry manufacturing process. For this purpose, simulations of a TSE are performed taking both process parameters and

rheological properties of the slurries into account. As a reference material, Li-ion battery slurries are considered due to their increasing development interest.^[1,12] For a detailed study of the geometrical effects, this publication focuses on the simulation of different process settings applied to individual modules or sections of the TSE mixing screw.

2.1. Material Properties

Lithium-ion batteries contain an active material (AM), a conductive material, a binder (Bi), and additives (Add). During the manufacturing process, a solvent is used to facilitate the mixing of battery components and improve handling for subsequent steps.^[2,4,13,14]

Depending on the application, different recipes of the electrode slurry and components are needed, resulting in a wide range of rheological properties that can be processed.^[2,13] In the case of cathodes, the active materials are mostly metal oxides, containing materials such as nickel, manganese, and cobalt, as in NMC and NCA.^[1,2] These components form a crystal structure with primarily rough round particles, making them more resilient toward strain compared to more fragile components such as carbon black (CB) agglomerates or graphite.^[1] Therefore, more dispersion energy can be applied. Accordingly, anodes and primarily graphite anodes, which are widely used for most applications, are more susceptible to particle rupture.^[9]

Battery slurries are processed at high solid contents from above 50%; at these concentrations, the fluid shows non-Newtonian rheological properties.^[14,15] The amount of solvent therefore has a great impact on the efficiency of the whole process because it determines the viscosity of the slurries affecting its processability.^[10,15] Although low solid contents are easier to handle, there is a tendency to use high solid contents because it significantly reduces the amount of thermal energy required to properly dry the electrodes after coating, which also has a major impact on the production costs.^[10] This increases the importance of a variable model that can respond to different slurry solids contents and compositions to ensure processability.

In order to match the material properties of the battery slurry, a viscous fluid is simulated in this article using a Newtonian fluid solver. This approach was implemented in order to calibrate the simulations. The battery slurry was then modeled using reference rheological data^[3,10,14,15] for NMC cathode slurries with around 70% solid content. A reference density of 2500 kg m⁻³ and an approximated average viscosity of 20 Pas were used to cover the expected rheological properties while processing.

2.2. Process Parameters

TSEs are high intensity mixing devices which offer great flexibility due to its modular construction. The material handling can be influenced through the rotational speed of the extruder screw and the flow rate. Accordingly, the proper control of these parameters enables the adaptation of the mixing performance to various material requirements. In addition, the screw geometry also has a great effect on the material processing features.

The extruder screw can be simplified into the arranging of multiples screw elements such as conveyors, kneaders, backward elements, and other special elements. The extruder investigated

in this work is the ZSK18 TSE from Coperion (Germany). The diameter of the screw (D_s) is 18 mm and the axis separation (a) of the twin screw equals to 15 mm. An overview of the investigated screw elements is shown in **Figure 1**.

Conveyors such as the C24-24 (1a) and C16-16 (1b) have the main functionality of conveying the materials in axial direction. They are therefore used to separate different extruder sections and also to enable mass transport along the screw. The main difference between conveyors is described by the pitch length, which describes the length of the screw that takes a whole rotation, and the element length. Both values result into different flow transport capacities. In this case, 24 and 16 mm are, respectively, both the pitch and element length for the evaluated conveyors. Kneaders (1f, 1e, 1d, 1c), on the other hand, are used for dispersion and intensive mixing, although kneaders also have a reduced conveying feature. Here, the main difference is the offset angle between the kneading blocks, as well as the width of the blocks. In this work, kneaders with an offset angle of 90° and 45° were evaluated, as for the 45° kneading block, three different kneading disk widths were considered, resulting in three kneaders of 8, 16, and 24 mm length. Finally, backward elements or left-handed screw elements are used to restrict mass transport by inducing a flow resistance working against the main extrusion direction, which derives in increase of pressure in the extruder.

In order to characterize the effects of different screw elements on the process, dimensionless numbers can be calculated to evaluate the process performance. This is achieved by correlating the process parameters with relevant materials properties for each screw module. Here, the screw element conveying effects are evaluated considering rheological properties of the battery slurry, as well as other process-relevant quantities such as the resulting pressure build-up, flow rate, and geometrical ratios. Consequentially, each screw element induces different flow profiles also depending on the process parameters. The dimensionless analysis was

introduced by Kohlgrüber and Pawloski^[16] and also has been well established on experimental and simulation investigations as in Eitzlmayr et al.^[17,18] and Matic et al.^[19] for various extruder types. In the present work, the focus is set on the dimensionless numbers \dot{V}^* (equation 1) and Δp^* (Equation 2).

$$\dot{V}^* = \frac{\dot{V}}{nD^3} \quad (1)$$

$$\Delta p^* = \frac{\Delta p D}{\eta n L} \quad (2)$$

The value \dot{V}^* is the dimensionless flow rate and describes the flow capacity of the screw element, as the ratio of the flow rate \dot{V} to the screw speed n and the screw diameter D . It also defines the process operational state correlating the process variables. Furthermore, Δp^* describes the dimensionless pressure number in terms of the pressure gradient Δp in relation to the material viscosity η , screw speed, and the ratio between screw diameter and the length of the screw element L . In case of Newtonian fluids, a linear relation between \dot{V}^* and Δp^* is obtained.^[16] The resulting equation can be written as Equation (3).^[19]

$$\Delta p^* = A_2 \left(1 - \frac{\dot{V}^*}{A_1} \right) \quad (3)$$

Here, characteristic values of the screw elements can be extracted such as A_1 and A_2 . A_1 describes the flow capacity of the screw element. A_2 describes the pressure features. Both are strongly subjected to the geometry parameters of the extruder such as the pitch length of the element, the diameter of the screw, and the gap size between screw and extruder wall.^[16] Nevertheless, as soon as those values are estimated, various operating states can be easily calculated and compared. This can be achieved experimentally or through simulations.

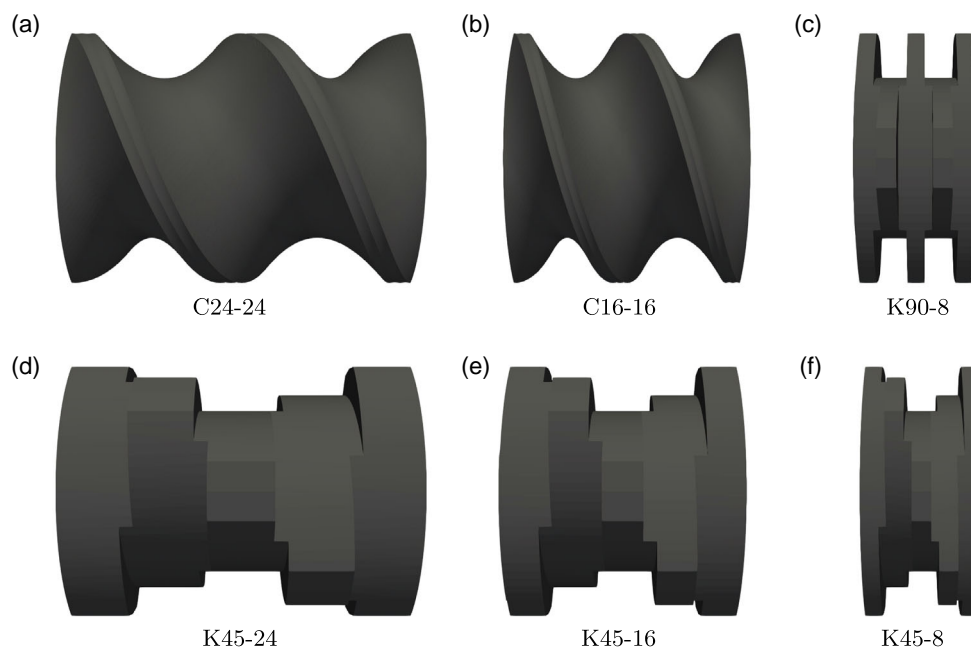


Figure 1. CAD models and overview of the analyzed screw elements. a) C24–24, b) C16–16, c) K90–8, d) K45–24, e) K45–16, and f) K45–8.

2.3. Simulation Setup

Continuous mixing steps in extruders can be found in a wide range of applications due to its versatility. However, depending on which material is being processed, the setup has to be adapted to match the process and product requirements. Usually, this is done iteratively or based on experience on similar products but always subject to long development times. In order to get a more detailed view of the working principle of extruders, a digital twin of the mixing module, focused on processing of battery materials, is developed. This is carried out based on computational fluid dynamics (CFD) simulations which are used to estimate flow states and pressures build-up zones during the extrusion process. Furthermore, the output of the simulations is used to find correlations between multiple process parameters and conduct a dimensionless analysis of the process to find scale-up numbers, as previously discussed.

The analysis of the flow states and mechanical effects performed by the different screw elements is carried out in this article through smoothed particle hydrodynamics (SPH) simulations. Here, the geometrical setup and the fluid flow calculations were implemented in the open-source software DualSPHysics.^[20] The SPH method offers great flexibility over conventional CFD methods because it is a meshless method and therefore the interaction between fluids and the complex moving geometries can be easily computed. SPH is based on the Lagrangian formulation of the continuity and momentum conservation equations and uses finite mass points, also called SPH particles, to simulate fluid flows. The particle interaction is then calculated using a kernel function; in this work, the fifth-order Wendland function is used due to its enhanced stability property.^[20] In addition, the software used is GPU compatible, allowing the simulation of more SPH particles without compromising computational cost.

The slurry in this publication is being considered as one phase. Accordingly, the fluid domain is discretized into SPH particles which contain the material properties of the slurry for calculation. As all SPH particles have the same size, the resolution of the simulation can be adjusted to improve the accuracy. This is given by the particle distance $dp = 0.15$ mm and the smoothing length $h = 1.5$ dp. These values have been found to provide the best results in terms of consistency and computational cost for the evaluated extruder. Moreover, the same simulation setup could be used to evaluate both fully and partially filled screw section without the need of multiphase solvers.

The calculations were performed using periodic boundary conditions which enable the simplification of the screw into single elements. Consequentially, only a smaller section of the extruder had to be simulated, reducing simulation time and therefore computational costs. This method is well established and has been used by various authors, such as in the work from Eitzlmayr et al. and Matic et al.^[18,19] However, by using a periodic boundary condition, the flow rate cannot be adjusted directly; therefore, the flow conditions in the simulation were induced by applying an external acceleration (a_{axial}) in flow direction, which decays in a pressure gradient Δp according to the equation $\Delta p = a_{axial}\rho L$.

The pressure field in the simulation is described through the weakly compressible approach. This approach is part of the many

formulations used in SPH and relies on the equation of state (EoS), Equation (4), for coupling the continuum field and the pressure field. The implementation in the solver and detailed formulation can be found in the work of Dominguez et al.^[20]

$$p = \frac{c_s^2 \rho_0}{\gamma} \left(\left(\frac{\rho}{\rho_0} \right)^\gamma - 1 \right) \quad (4)$$

The equation describes the local pressure p through the local density ρ according to a reference density ρ_0 , a material parameter γ , and the speed of sound c_s . The latest is on behalf of simulations defined as a numerical speed of sound.^[20] In order to achieve a stable simulation, the criteria proposed by Morris et al.^[21] were used to determine the speed of sound needed. Here, a higher c_s value would increase stability but also increase computational cost. It was found that for a reference rotational speed of 60 RPM, a speed of sound of 40 m s^{-1} produces a stable simulation with almost no SPH particles leaving the fluid domain. Finally, a material parameter of 7 is commonly used for water^[20] and therefore was also used in this work as a reference.

The flow conditions in the extruder can be described by the Reynolds number. This is defined as $Re = nD^2\rho/\eta$ and depends on the screw speed n , the screw diameter D , and the material properties, such as viscosity η and density ρ . Eitzlmayr et al.^[18] showed that for TSEs the Reynolds number has to be less than 10 ($Re \ll 10$) in order to achieve creeping-flow conditions. The reference screw speed used in this article equals to 60 RPM, resulting in a Reynolds number of $Re \approx 0.04[-]$ fulfilling the criterion.

2.3.1. Numerical Shear Rate

The mixing performance in TSEs is encouraged through the rotation and interaction between both screws. Thus, depending on the screw configuration, the dispersion degree and the mechanical load of the materials can be adapted to various products requirements. Regarding dispersion, particles during extrusion flow following near to random pathways induced by the complex geometry of the screw elements. Consequentially, during extrusion particles in the slurry will hold various velocities depending on its position. This can be translated into different strain rates, considering the velocity fields induced by the high rotational speeds of the screw and by the conveying features of the extruder.

Given a shear field acting on structures such CB agglomerates or graphite, besides having a significant effect on the viscosity due to the shear thinning nature of the battery slurries, it is also important to be characterized because it causes breakage of large structures in the slurry.^[8,9] As a consequence, the dispersion of conductive materials across the battery is affected. This can lead to an enhancement or even loss of conductivity in the battery cell.

Typically, the shear rate $\dot{\gamma}$ in single-screw extruders is defined as $\dot{\gamma} = \pi Dn/h$.^[16,22] Here, the shear rate only depends on the screw speed n and geometrical aspects of the screw such as the diameter D and the channel depth h . However, in the case of TSEs, the pressure flow also has to be considered.^[22] The shear rate is calculated in this work using Equation (6).^[20] This is given by the magnitude of the shear rate tensor, Equation (5), which is calculated through the trace function $\text{tr}(\dot{\gamma})$. Moreover, the shear rate tensor is obtained out of the velocity field \vec{v} , based on the strain rate tensor.

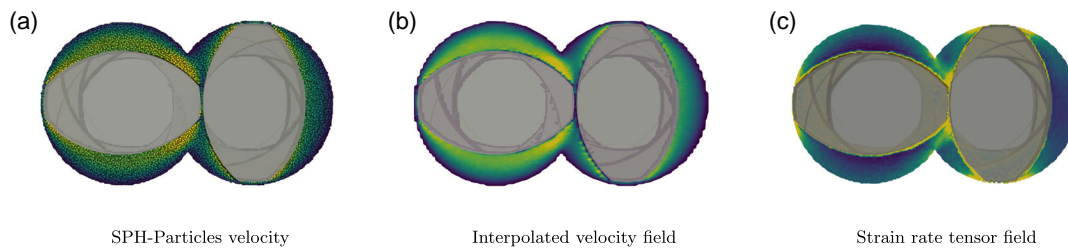


Figure 2. Steps for strain rate calculation. a) SPH-particles velocity, b) interpolated velocity field, and c) strain rate tensor field.

$$\dot{\gamma} = \nabla \vec{v} + \nabla \vec{v}^T \quad (5)$$

$$|\dot{\gamma}| = \sqrt{\frac{1}{2}(\text{tr}(\dot{\gamma}^2) - \text{tr}(\dot{\gamma}^2))} \quad (6)$$

Here, the shear rate $\dot{\gamma}$ in a given extruder section strongly depends on the flow profiles, as a function of the velocity fields, which are directly influenced by the process parameters and the resulting flow states. The velocity field is then obtained from the simulations, where for each SPH particle the velocity and position is tracked and stored. The gradient of the velocity field is calculated after interpolating the simulation domain as shown in **Figure 2**. The strain tensor is accordingly calculated based on the interpolated velocity field to extract the local shear rate values as previously discussed.

3. Results and Discussion

The aim of this work is to evaluate the effects of various flow conditions that may occur in the extruder as a result of both the operational setup and the module geometry on the shear rate. This is carried out in order to quantify the effects on the resulting mechanical stress at each screw element in the extruder.

3.1. Pressure Characteristics

Considering a fully filled screw section, the pressure either drops or builds up in the extruder section. This relies mostly on the screw configuration, for example, by using left-handed screw elements, or on the process setup. Consequentially, the material flow is retained longer at the screw section or even suffers overflow. In this work, four different flow conditions for fully filled extruder section were simulated by setting an axial pressure gradient with, respectively, $a_{\text{axial}} = -400, -100, 0,$ and 100 m s^{-2} and following the equation $\Delta p = a_{\text{axial}} \rho L$. Accordingly, the resulting velocity fields are obtained out of the simulations. Finally, to determine the resulting flow rate through the extruder section at a given pressure setup, the axial component of the velocity field was considered.

In order to validate the simulation setup, simulation data^[18] found in the literature are compared to the results obtained in this work. Here, matching geometries for both the literature and the present work are considered. Consequentially, a comparison of the pressure lines based on the conveying elements C24 and C16 was accomplished, as shown in **Figure 3**.

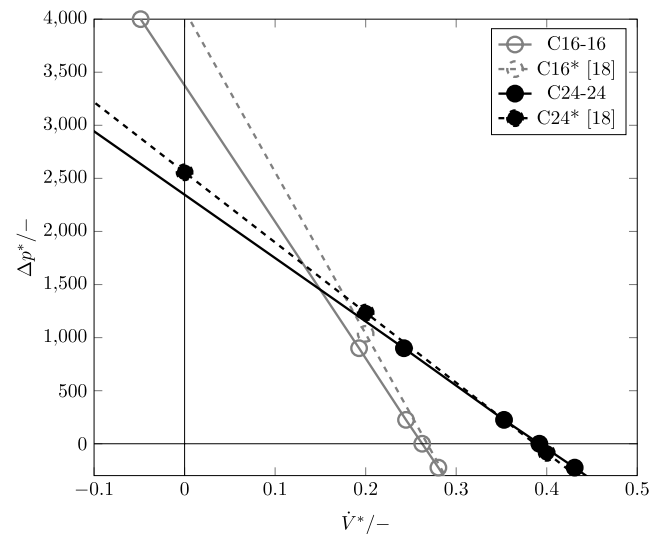


Figure 3. Comparison of the simulated pressure profiles with reference simulation data (*) for the conveying screw elements C24-24 and C16-16.

The simulation results for both C24-24 and C16-16 screw elements show a great agreement with the literature reference data. Especially for the flow capacity (A_1) of the screws, where it can be observed that the calculated values based on the simulated data agree with the reference data. On the other hand, the pressure number (A_2) showed a slight deviation for both C24-24 and C16-16 compared to the reference simulation data. This can be explained through the dependency between A_2 and the clearance between screw and barrel wall, which can be affected by the accuracy of the screw and barrel geometry generation in the software. Nevertheless, the estimated values A_1 and A_2 , as well as the slope of the pressure line are equivalent to the validation data and also exhibit the expected linear correlation for the simulated Newtonian slurries.

The same simulation setups and procedure can be applied to others screw elements, to calculate further pressure features for various screw elements. **Figure 4** shows the resulting pressure characteristics lines for the kneaders and conveyors evaluated in this work.

For all screw elements, the same four flow conditions were simulated. Here, all of the evaluated elements showed a linear relation and could be fitted properly using Equation (3). The different slopes of the lines characterize the features of each screw element and are valid for fully filled screw sections. Each pressure

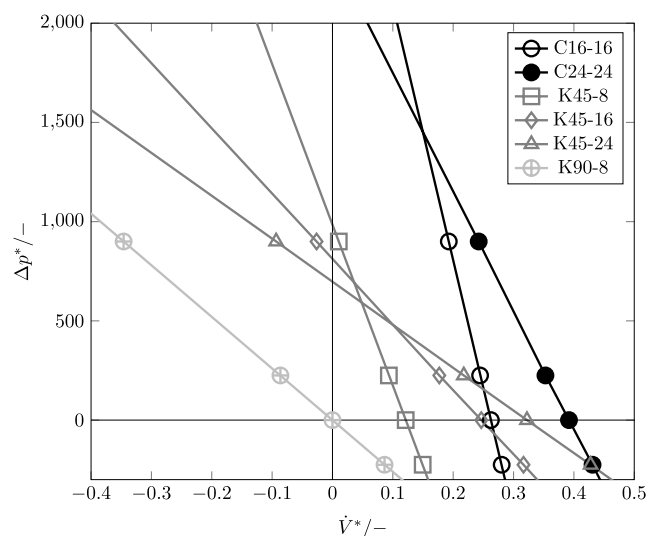


Figure 4. Pressure characteristics lines of singles screw elements (ZSK18) based on SPH simulations.

line is used to describe the resultant flow states that occur during extrusion depending on the process parameters and the screw configuration. If \dot{V}^* becomes higher than A_1 , a pressure loss occurs due to overflowing of the screw element. For \dot{V}^* values between 0 and A_1 , pressure builds up in the screw section. If the pressure increases higher than A_2 , backflow is expected. The axes intersection values for each screw element could be reached by extrapolating the data. The corresponding values for A_1 and A_2 are summarized in Table 1.

As expected, longer screw elements exhibit a greater flow capacity resulting in higher A_1 values. In the case of the kneaders with 45° offset (K45), it can be observed that thinner disks lead to higher A_2 values, meaning that the flow resistance is higher. The same effect can be observed in conveyors where less pitch length also leads to a higher flow resistance and therefore higher pressure development. Finally, kneaders with 90° offset (K90) do not exhibit a conveying feature. In this case, the pressure features are described through A_0 , which is given by the slope of the graph.

3.2. Local Shear Rate

In order to be able to predict or induce a specific mechanical stress in the extruder, calculations of the shear rate distribution caused by different screw elements and process parameters are

Table 1. Overview of the pressure key figures A_1 and A_2 for the simulated ZSK18 extruder based on SPH simulations.

Element	A_1	A_2
C16–16	0.2625	3375.7
C24–24	0.3919	2344.0
K45–8	0.1213	983.7
K45–16	0.2466	811.3
K45–24	0.3222	697.3
K90–8	$A_0 = 2601.7$	

carried out. First, the effects of the operational setups on the local shear rate in fully filled screw section were analyzed for various screw elements. Based on Figure 4, two operational setups with the same flow rate and rotational speed for similar elements were extracted. Here, C24–24 and K45–24 both at $a = 100 \text{ m s}^{-2}$ and C16–16 at $a = -100 \text{ m s}^{-2}$ and K45–16 at $a = 0 \text{ m s}^{-2}$ were considered, as for both screw element pairs the length is, respectively, equal and the flow rates are similar. This is shown in Figure 5. Here, the shear rate values of the whole simulation domain for ten time steps were evaluated, due to periodical fluctuations in the velocity fields induced mainly by the interaction between the screws. This represents 0.5 s of real time. The calculations were executed accordingly after reaching a steady-state flow regarding the velocity fields for each setup. Additionally, the effects of the flow rate on the shear rate for a single-screw element are evaluated. This is based on the kneader K45–24 for simplicity.

According to Figure 5a, the effects of the flow rate on the shear rate are more appreciable for low values of the shear rate. Moreover, comparing two similar screw sections with the same length at the same process setup, Figure 5b, it is noticeable that kneaders on average exhibit slightly more shear rates than conveyors. However, this is more appreciable for longer screw elements. This evaluation accounts for fully filled screw sections.

Depending on the screw configuration and the process setup, if no pressure builds up in an extruder zone, only a partial filling of the screw section occurs. Figure 6 shows the density distribution of the calculated shear rate based on the K45–8 module for four filling ratios of the screw section. It illustrates the effects of the filling ratio of a single kneading module on the shear rate.

It can be observed that for the evaluated fill ratios, all distribution functions cover a similar range of shear rates. Beyond that, it denotes that low shearing values are more present at lower fill ratios and, for instance, higher shear rates also occur at lower fill ratios. As a result, low fill ratios exhibit a wider distribution function compared to the more concentrated distributions at higher fill ratios. Beyond that, it denotes that the peak of the distributions differs for all calculations, some even showing various peaks. The transition of peak values in the density distribution functions can be explained through the placement of the material across the screw section as the extruder fills up for the calculated screw speed. The fluid distribution and the resulting material strain values for the investigated setups are shown in Figure 7. At low fill ratios, the material is predominately affected by the outer parts of the kneading disks and the barrel, causing high shear rates in the material. As the fill ratio increases more material is affected by this interaction; however, lower shear rate values start gaining dominance because more material fills up the hollow parts of the screw section. In addition, the material tends to fill up first one half of the extruder section and then the other, causing an uneven distribution of the material.

A similar analysis can be accomplished when comparing the distribution of the shear rate for kneading blocks with the same offset angle but different disk width. Figure 8 illustrates the effects of the width of kneading blocks based on three variants of the K45 screw element, accordingly K45–8, K45–16, and K45–24. In addition, the shear rate distributions show a comparison between fully (100%) and partially (25%) filled extruder sections.

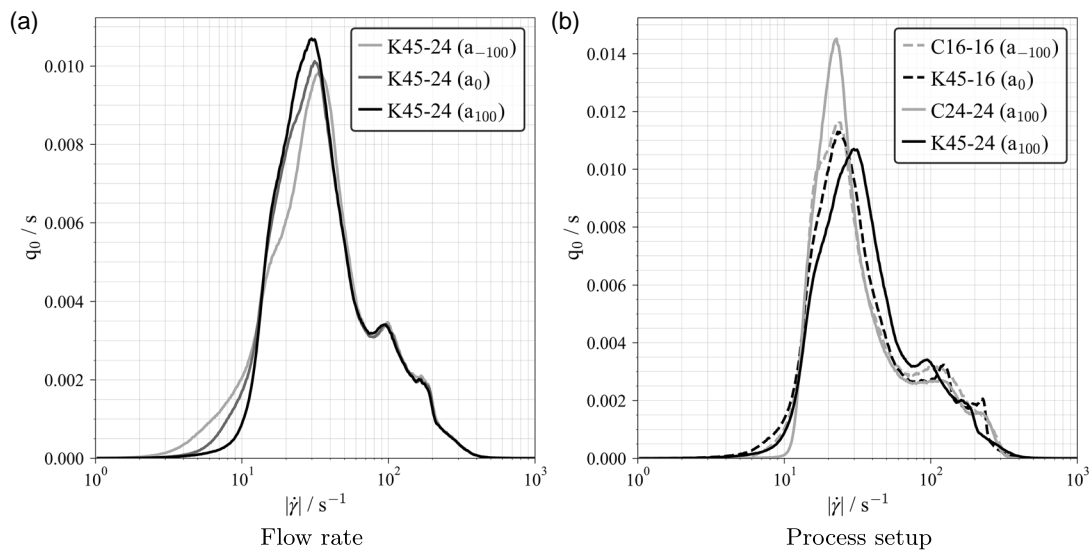


Figure 5. Shear rate distribution plot for different operational setups: a) flow rate and b) process setup.

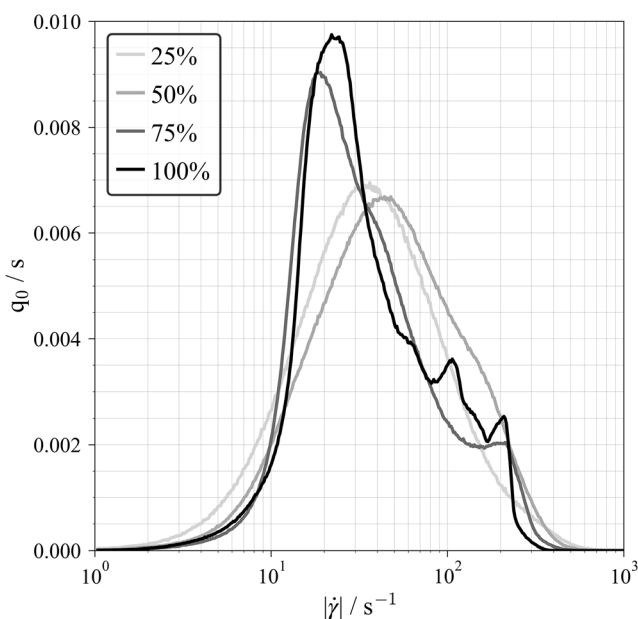


Figure 6. Density distribution plot of the shear rate by different filling ratios in the K45-8 module.

As expected, it is shown that in the case of a 45° offset kneading block, a wider disk induces a slightly higher average shear rate compared to thinner kneading disks. This effect is more evident in low filling ratios of the modules. These observations also fulfilled the statements found in the literature, where wider kneaders exhibit a higher shear effect regarding dispersion while inducing a lower mixing effect.^[16] In addition, the shifting of the peak of the shear rate distribution caused by the filling up of the extruder section is also present.

Finally, the screw rotational speed was also considered for this evaluation. Following $\dot{\gamma} = \pi Dn/h$, applying a reference screw

speed of 60 RPM results in a mean shear rate value of 17.671 s^{-1} . This value agrees well with the peak values of the distribution at a filled extruder section for the already introduced kneaders. With this in mind, a study showing the relevance of the rotational speed of the twin-screw was conducted. Here, the shear rate values were calculated based on the simulation results using a rotational speed of 60 and 300 for the kneaders K90-8 and K45-8. The resulting shear rate distributions are resumed in **Figure 9**. Accordingly, K90-8 was considered for this evaluation due to its nonconveying feature. Moreover, the effects of partial filling in a screw section are more appreciable in other kneaders as in K45-8.

It can be observed that not only the shear rate increases with the speed but also its density distribution reaches a wider range, meaning that at higher rotational speed, the material can experience both low and higher shear rates, depending on its location. On the other hand, at lower rotational speed a more narrow stress can be expected. Moreover, the peak values of the distributions for higher screw rotational speed exhibit in each configuration a near proportional transition to the increase of screw speed. Regarding K90-8, an increment of the peak shear rate from 35.124 to 156.581 s^{-1} was calculated. As for K45-8, an increment of the peak shear rate from 21.687 to 131.208 s^{-1} for the fully filled screw section and 35.693 to 215.943 s^{-1} for the partially filled (25%) screw section was obtained. This can be compared to the reference (single-screw) shear rate value of 17.671 and 88.357 s^{-1} respectively, for the calculated setups, corresponding to a channel depth of 3.2 mm, where a linear increase of the shear rate is expected. By this means, the effects of the interaction of the two screws in the TSE compared to a single-screw configuration are appreciable. Moreover, the raise in the shear rate distributions due to higher rotational speeds corresponds to the expectations.

Based on these evaluations, particles in the fluid experience different stress and strain conditions depending on where they are located across the extruder. This also is affected by the filling

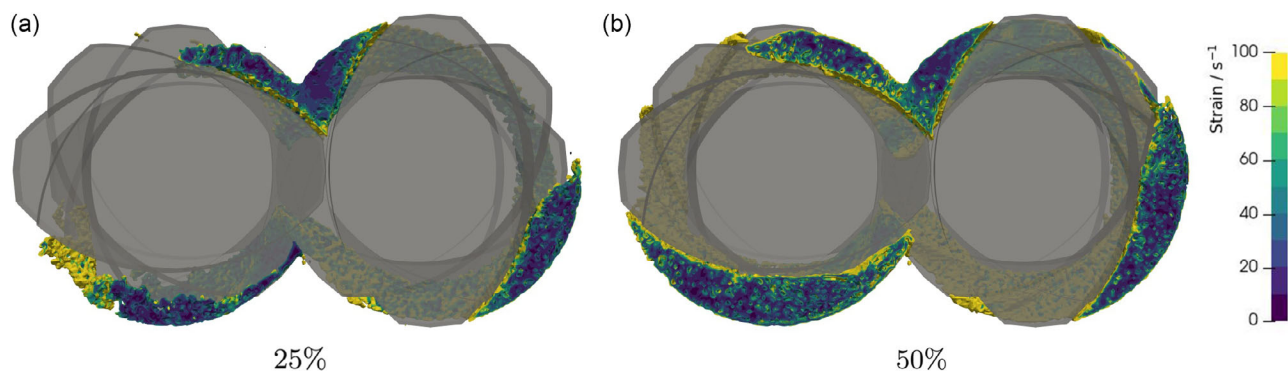


Figure 7. Spatial distribution of material and strain (magnitude) in a kneading block (K45-8) for low filling ratios at $n = 60$ RPM. a) 25% and b) 50%.

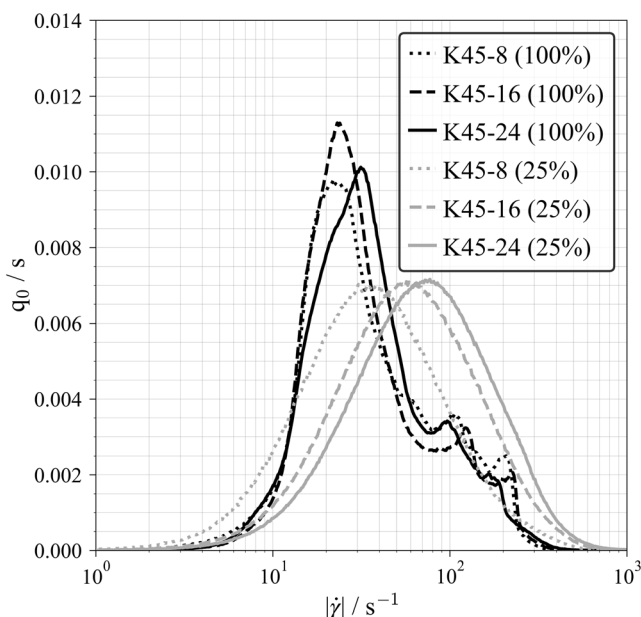


Figure 8. Comparison of the shear rate density distribution for partial and fully filled K45-8, K45-16, and K45-24 kneading modules.

degree and the geometry, but mostly by the screw rotation. Moreover, the movement of the particle in each screw section also has a great impact on the duration of the strain load that a certain particle holds. As a result, depending on the initial conditions of the process parameters the mechanical stress induced by the extruder can be quantified. This can be used to better assess quality changes in battery slurries during production, such as controlling changes in particle size distribution by generating sufficient critical stress for particle breakage.

4. Conclusion

In this article, a numerical investigation of the continuous processing of viscous battery slurries in a TSE was conducted. This was done in order to analyze the material behavior inside the extruder and to be able to develop possible screw configurations

adapting it to new material requirements. The investigation showed that in order to predict changes in the production quality of battery slurries, a wide range of process parameters have to be considered. By modeling the slurry using the SPH method, a fluid flow simulation framework for the assessment of different parameter configurations was generated. Hence, an evaluation of the main interaction features between various screw elements and the slurries is conducted. Supported by simulations of the material flowing through single-screw sections, a characterization of the local mechanical strain is achieved. Moreover, a dimensionless number analysis for the evaluated extruder was accomplished. The generated dimensionless number correlations were compared to reference literature data for validation of the simulations.

The pressure characteristics for each evaluated screw element are successfully calculated from the simulation data presented in this article. It could be observed that the pressure lines based on dimensionless numbers agreed well with reference data found in the literature for the same TSE (ZSK18), especially considering the flow capacity factor A_1 . However, a small deviation regarding the pressure factor A_2 compared to the reference data was obtained. This is explained through the dependency of the pressure factor to the clearance between screw and barrel due to the possible inaccuracy of the software used for the geometry generation. The simulation setup was then used to determine further screw elements pressure and flow features.

An analysis of the effects of process parameters on the mechanical strain inside an extruder was carried out. Here, a numerical investigation of the local shear rate for partially and fully filled screw sections was conducted, comparing various screw elements of the extruder. The shear rate tensor is obtained based on calculations of the velocity field in single modules. At first, fully filled screw sections were considered. Comparing two different screw types of the same ratios (L/D), similar shear rates could be observed. By simulating a partial filling state in the extruder, the material behavior was analyzed in each section at different process setups. At a reference screw speed of 60 RPM, an uneven material distribution occurs which derived into an uneven strain of the material. As a consequence, the density distribution functions exhibit various peak values which could be explained through material location at different fill ratios of the extruder sections. Accordingly, changes into the fill ratio of an extruder section cause different shear profiles and therefore

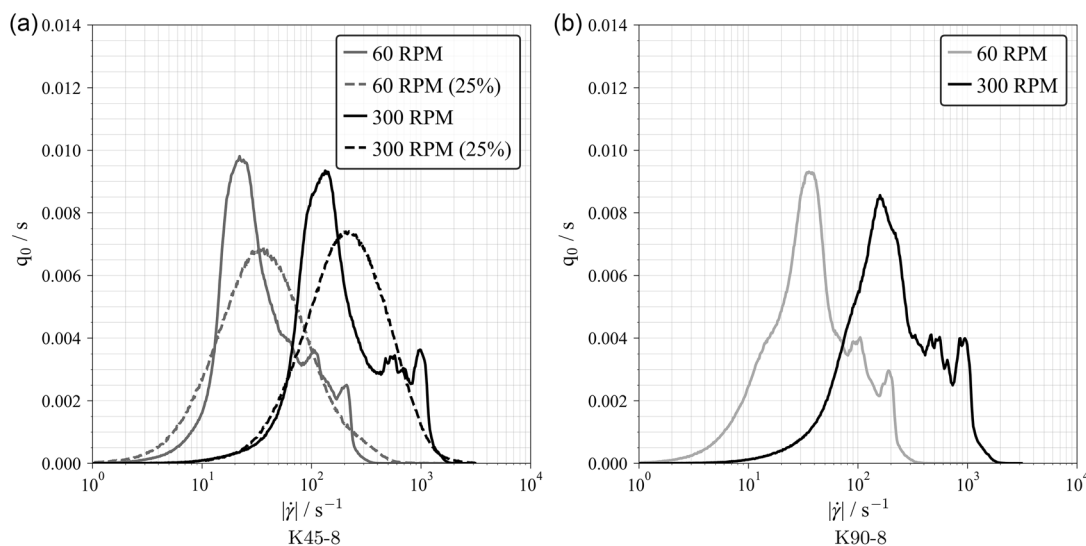


Figure 9. Comparison of the shear rate density distribution for the kneading block K90–8 and K45–8 with variation of the rotational speed. a) K45–8 and b) K90–8.

causes a strong variation in the local shear rates. Regarding kneading blocks, low-to-moderate filled sections feature higher shearing because the material tends to gather closer to the screw/barrel clearance. For higher fill ratios, material filled first one half of the extruder, affecting the average strain into lower shearing. This occurs because more material has to be transported and it also fills up wider cross sections first.

This article denotes the effects of the resulting flow profiles generated by various process parameter combinations, as well as geometrical features of the screw elements, on the local mechanical stress in the extruder, by analyzing changes in the shear rate distribution. Furthermore, it is shown that the mechanical stress induced by the extruder can be quantified and controlled through proper parameter setups. Accordingly, critical stress for particle breaking can be accomplished to manage changes in the particle size distribution. Moreover, the analysis helps to evaluate the quality changes of the battery slurries during production. Nevertheless, the time in which the material is exposed to this mechanical stress also has an influence on the efficiency of the process. Therefore, the dependency of these profiles to the residence time should be considered for accurate particle mixing and processing analysis in extruders.

Acknowledgements

Funding and support by the Federal Ministry of Education and Research (Bundesministerium für Bildung und Forschung [BMBF]) and Project Management Jülich (Projektträger Jülich [PTJ]) throughout the research cluster InZePro under the project 03XP0369A are highly acknowledged. Moreover, the authors acknowledge support by the state of Baden-Württemberg through bwHPC.

Open Access funding enabled and organized by Projekt DEAL.

Conflict of Interest

The authors declare no conflict of interest.

Data Availability Statement

The data that support the findings of this study are available from the corresponding author upon reasonable request.

Keywords

electrode slurry, Li-ion batteries, shear rate profiles, smoothed particle hydrodynamics, twin-screw extruder

Received: December 26, 2022

Revised: February 14, 2023

Published online:

- [1] N. Nitta, F. Wu, J. T. Lee, G. Yushin, *Mater. Today* **2015**, *18*, 252.
- [2] J. Li, J. Fleetwood, W. B. Hawley, W. Kays, *Chem. Rev.* **2022**, *122*, 903.
- [3] M. Keppeler, S. Roessler, W. Braunwarth, *Energy Technol.* **2020**, *8*, 2000183.
- [4] J. Entwistle, R. Ge, K. Pardikar, R. Smith, D. Cumming, *Renew. Sustain. Energy Rev.* **2022**, *166*, 112624.
- [5] A. C. Ngandjong, A. Rucci, M. Maiza, G. Shukla, J. Vazquez-Arenas, A. A. Franco, *The J. Phys. Chem. Lett.* **2017**, *8*, 5966.
- [6] A. Rucci, A. C. Ngandjong, E. N. Primo, M. Maiza, A. A. Franco, *Electrochim. Acta* **2019**, *312*, 168.
- [7] J. K. Mayer, L. Almar, E. Asylbekov, W. Haselrieder, A. Kwade, A. Weber, H. Nirschl, *Energy Technol.* **2020**, *8*, 1900161.
- [8] E. Asylbekov, R. Trunk, M. J. Krause, H. Nirschl, *Energy Technol.* **2021**, *9*, 2000850.
- [9] V. Wenzel, H. Nirschl, D. Nötzel, *Energy Technol.* **2015**, *3*, 692.
- [10] M. Haarmann, W. Haselrieder, A. Kwade, *Energy Technol.* **2020**, *8*, 1801169.
- [11] H. Dreger, H. Bockholt, W. Haselrieder, A. Kwade, *J. Electron. Mater.* **2015**, *44*, 4434.
- [12] G. Zubi, R. Dufo-López, M. Carvalho, G. Pasaoglu, *Renew. Sustain. Energy Rev.* **2018**, *89*, 292.

- [13] C. D. Reynolds, S. D. Hare, P. R. Slater, M. J. H. Simmons, E. Kendrick, *Energy Technol.* **2022**, *10*, 2200545.
- [14] W. Bauer, D. Nötzel, *Ceram. Int.* **2014**, *40*, 4591.
- [15] L. Ouyang, Z. Wu, J. Wang, X. Qi, Q. Li, J. Wang, S. Lu, *RSC Adv.* **2020**, *10*, 19360.
- [16] K. Kohlgrüber, in *Co-Rotating Twin-Screw Extruders Fundamentals*, 1st ed., Hanser Publications, Cincinnati, OH **2019**.
- [17] A. Eitzlmayr, J. Khinast, G. Hörl, G. Koscher, G. Reynolds, Z. Huang, J. Booth, P. Shering, *AIChE J.* **2013**, *59*, 4440.
- [18] A. Eitzlmayr, J. Matić, J. Khinast, *AIChE J.* **2017**, *63*, 2451.
- [19] J. Matić, A. Witschnigg, M. Zagler, S. Eder, J. Khinast, *Chem. Eng. Sci.* **2019**, *204*, 257.
- [20] J. M. Domínguez, G. Fourtakas, C. Altomare, R. B. Canelas, A. Tafuni, O. García-Feal, I. Martínez-Estévez, A. Mokos, R. Vacondio, A. J. C. Crespo, B. D. Rogers, P. K. Stansby, M. Gómez-Gesteira, *Computat. Part. Mech.* **2021**.
- [21] J. P. Morris, P. J. Fox, Y. Zhu, *J. Comput. Phys.* **1997**, *136*, 214.
- [22] B. Vergnes, *Polymers* **2021**, *13*, 304.